

# Automated sample-scanning methods for radiation damage mitigation and diffraction-based centering of macromolecular crystals

Mark C. Hilgart,<sup>a\*</sup> Ruslan Sanishvili,<sup>a</sup> Craig M. Ogata,<sup>a</sup> Michael Becker,<sup>a</sup> Nagarajan Venugopalan,<sup>a</sup> Sergey Stepanov,<sup>a</sup> Oleg Makarov,<sup>a</sup> Janet L. Smith<sup>b</sup> and Robert F. Fischetti<sup>a</sup>

<sup>a</sup>Biosciences Division, Argonne National Laboratory, 9700 South Cass Avenue, Bldg 436D, Argonne, IL 60439, USA, and <sup>b</sup>Life Sciences Institute, Department of Biological Chemistry, University of Michigan, Ann Arbor, MI 48109, USA. E-mail: mhilgart@anl.gov

Automated scanning capabilities have been added to the data acquisition software, *JBluIce-EPICS*, at the National Institute of General Medical Sciences and the National Cancer Institute Collaborative Access Team (GM/CA CAT) at the Advanced Photon Source. A ‘raster’ feature enables sample centering *via* diffraction scanning over two-dimensional grids of simple rectangular or complex polygonal shape. The feature is used to locate crystals that are optically invisible owing to their small size or are visually obscured owing to properties of the sample mount. The raster feature is also used to identify the best-diffracting regions of large inhomogeneous crystals. Low-dose diffraction images taken at grid positions are automatically processed in real time to provide a quick quality ranking of potential data-collection sites. A ‘vector collect’ feature mitigates the effects of radiation damage by scanning the sample along a user-defined three-dimensional vector during data collection to maximize the use of the crystal volume and the quality of the collected data. These features are integrated into the *JBluIce-EPICS* data acquisition software developed at GM/CA CAT where they are used in combination with a robust mini-beam of rapidly changeable diameter from 5  $\mu\text{m}$  to 20  $\mu\text{m}$ . The powerful software–hardware combination is being applied to challenging problems in structural biology.

## 1. Introduction

The mini-beam capability developed at GM/CA CAT (National Institute of General Medical Sciences and the National Cancer Institute Collaborative Access Team) has enabled both data collection from very small crystals as well as selective irradiation of larger crystals (Sanishvili *et al.*, 2008; Fischetti *et al.*, 2009). The small crystals that the mini-beam makes accessible to data collection (typically 10  $\mu\text{m}$  in size or smaller) are often optically obscured and impossible to center by standard optical methods. This problem was initially overcome by manual searching across the sample mount with a small X-ray beam. Similarly, spreading radiation damage among several sites on a crystal during collection of a data set also was carried out manually by translation of the sample and re-centering on an unexposed site (for example, Rasmussen *et al.*, 2007). These manual operations are labor intensive and slow, and they divert the experimenter from other tasks such

as sample evaluation and data processing. Therefore, two automated sample-scanning methods were developed and added to the GM/CA data-acquisition software, *JBluIce-EPICS* (Stepanov *et al.*, 2011).

The first method, known as rastering, is a grid search technique for finding small invisible crystals and for mapping crystal quality. Diffractive rastering in macromolecular crystallography was first reported as part of an auto-centering capability with a large beam at the Stanford Synchrotron Radiation Lightsource (SSRL) (Song *et al.*, 2007). Implementations with small beams at the Diamond Light Source and the European Synchrotron Radiation Facility (ESRF) have been published (Aishima *et al.*, 2010; Bowler *et al.*, 2010), and are also available at other beamlines at the Advanced Photon Source (APS). Preliminary reports of the initial GM/CA rastering implementation have been published (Cherezov *et al.*, 2009; Stepanov *et al.*, 2011). Here we report the full implementation of rastering including a simple rectangular

grid and multiple polygons, which speed up the procedure and reduce radiation exposure to samples. We also describe the rastering user interface, which was designed to provide maximum simplicity and convenience.

The second method, known as vector collect, automatically moves the sample along a user-defined vector during data collection to mitigate the effects of radiation damage. A similar method, known as helical data collection, was first implemented at the ESRF (Flot *et al.*, 2010), and later integrated with the data acquisition program *MxCuBE* and thus made available to general users (Gabadinho *et al.*, 2010). The GM/CA-CAT version reported here was designed based on input from many users of the raster feature. The vector-collect feature is implemented as an additional option in the *JBluIce-EPICS* data collection interface and, like rastering, maintains the successful design themes of the *BluIce* developed at SSRL (McPhillips *et al.*, 2002).

The new GM/CA CAT automation features were enabled by a high degree of reproducibility and stability in the beamline optics, the beam delivery and the sample-positioning systems, which together allow a sample to be positioned repeatedly to within 1  $\mu\text{m}$  and allow the beam size to be changed on demand without needing to re-align the beamline (Fischetti *et al.*, 2007, 2009). The reliability of the mini-beam and the capability for users to rapidly change beam diameter between 5  $\mu\text{m}$ , 10  $\mu\text{m}$  and 20  $\mu\text{m}$  led to a plethora of user suggestions for more powerful features, which are embodied in the systems described here. A mature version of the rastering feature has been available to all users since June 2008 and of the vector-collect feature since February 2010. The polygon rastering feature was introduced in January 2011. Both methods have matured and continue to evolve in response to many user suggestions.

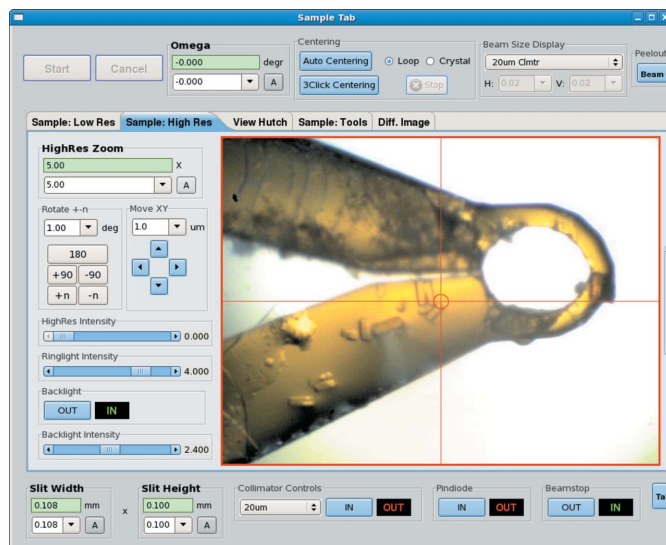
## 2. Polygon diffraction rastering

The diffraction rastering feature is applicable to individual micro-crystals, fields of micro-crystals, and larger crystals. After centering a sample (an individual large or small crystal or a field of microcrystals), the user defines a search area and a cell size, along with other collection parameters; then *JBluIce-EPICS* moves each cell in the search area into the beam and records a diffraction image (Fig. 1). Images are optionally processed for real-time quality feedback. Rastering can scan almost as fast as data collection itself, while manual rastering is slow, tedious and error-prone.

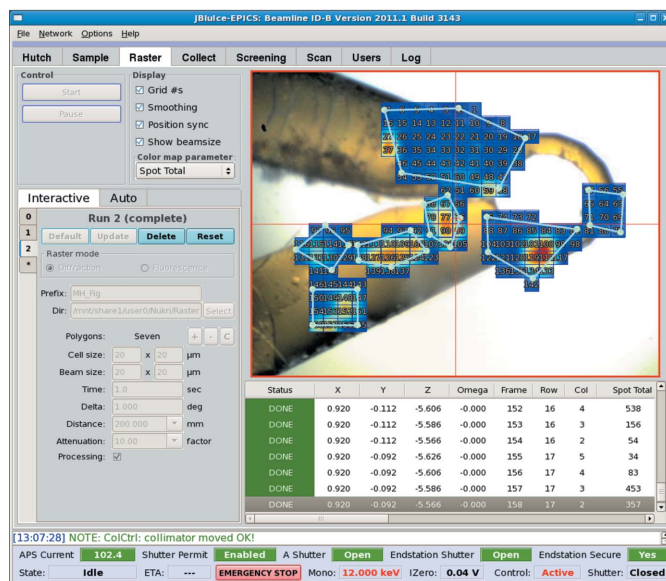
The development of the diffraction rastering feature at GM/CA CAT was initially motivated by the need to find small invisible crystals (Cherezov *et al.*, 2007, 2009). The feature is critical for membrane protein crystals grown in a lipidic cubic phase because the optical image generally lacks contrast between crystals and lipidic cubic phase (Caffrey & Cherezov, 2009). The GM/CA rastering feature with a mini-beam has been critical for locating and collecting data from invisible membrane protein crystals grown in lipidic cubic phases (Jaakola *et al.*, 2008; Wu *et al.*, 2010; Chien *et al.*, 2010; Xu *et al.*, 2011). Also, GM/CA-CAT rastering has been used successfully

to probe individual crystals within fields of micro-crystals that are mounted *en masse* and to identify and center one or more candidates for data collection (Leonard *et al.*, 2011).

The GM/CA diffraction rastering feature proved to be equally useful for mapping the quality of larger samples with the intent of collecting diffraction data from their best-diffracting regions (Sanishvili *et al.*, 2008; Jensen *et al.*, 2010).



(a)



(b)

Figure 1

Diffraction rastering of multiple polygons. (a) A clear view of the sample after centering. (b) The user outlined each of several potential crystals with a polygon. The polygons were filled with cells of user-defined size that is matched to the selected 20  $\mu\text{m}$  mini-beam. In the process of rastering, the sample is translated to center each cell in the grid at the beam position and a diffraction image is recorded. In this case, image processing is enabled and the results table is populated with quality indicators for each cell. Only 'Spot Total' is shown here; other quality indicators can be viewed by moving the slide bar to the right, and column widths can be adjusted to keep the user-favored quality indicator in view. Each cell in the sample viewer is colored according to the user-selected quality indicator on the left. Note that run parameters (lower left) cannot be changed after the rastering run is started.

Many large crystals are not of uniform diffraction quality and benefit from a single or multiple raster runs with the 5  $\mu\text{m}$ , 10  $\mu\text{m}$  or 20  $\mu\text{m}$  mini-beam to locate the most promising sites or regions for data collection. This strategy is most frequently used with crystals for which a larger beam results in smeared or split diffraction spots or reveals unacceptably high mosaicity. In many cases, smaller volumes of the sample are more perfectly crystalline, and the benefits of improved spot shape and mosaicity outweigh the disadvantage of irradiating fewer unit cells with a mini-beam. The GM/CA diffraction rastering feature is also used to isolate a single-crystal from a multiple-crystal cluster and to ensure that the beam intercepts only one crystal during data collection (Gehret *et al.*, 2011). Poor spot shapes, non-uniform mosaicity and split or multiple crystals are common problems. The mini-beam together with diffraction rastering have ‘rescued’ many such samples from the dustbin.

Additionally, the diffraction rastering tool is used to center crystals that are visible but are optically obscured by the mounting solution or by the mounting material. The image of a crystal may be optically distorted or subject to refractive effects if the volume of mounting solution is larger than the crystal. Crystals mounted in loops can be difficult to see when oriented with the plane of the loop along the viewing direction. Both effects greatly complicate optical centering. As X-rays are not distorted by these effects, diffraction-based centering is a more robust method for crystal centering.

Finally, the effects of photoelectron escape into adjacent unirradiated regions of the sample can be significant with smaller beams (Sanishvili *et al.*, 2011). If 1  $\mu\text{m}$  or smaller-diameter beams come into broad use, the polygon raster feature may be an important tool for avoiding irradiation of any regions of the sample that are not of potential interest for data collection.

### 2.1. Polygon diffraction rastering implementation

Diffraction rastering is organized into runs. A raster run is defined by a list of user-specified parameters to set up the beamline and the raster grid. The results of rastering with the set-up parameters are associated with the run and can be accessed after completion of the run, allowing the sample to be returned to any position in any stored run for data collection or further analysis. *JBluIce-EPICS* can store the parameters and results for up to 16 raster runs.

For each run, the grid layout is displayed over the live high-resolution camera video from the on-axis sample visualization system (Fig. 1). This is crucial to allow the user to match grid and cell sizes to the portions of the sample to be searched. As the user enters new grid parameters, the grid display is updated immediately.

The highly flexible search area can include multiple regions that may be rectangles or complex polygons. A simple definition consists of a single rectangular grid, which is created by choosing the rectangle’s opposite corners with the mouse or by entering the width and height of a rectangular grid that is centered on the current beam position and aligned with the

camera axes. This is useful for fine-stepping a single grid cell from a previous coarse raster run, since the cell being fine-stepped is also aligned and its size is known.

Polygonal rastering of one or more search areas allows the user to define precisely which parts of the sample to raster. The implementation is simple and flexible. The user clicks multiple points that define and connect the vertices of a polygon (Fig. 1) and then clicks ‘Done’. Rectangular cells are then calculated to fill the polygon. Multiple polygons can be defined to allow disconnected regions of the sample to be rastered in a single run. Depending on the crystal shape and orientation, polygon rastering may significantly reduce the number of diffraction images needed to characterize a sample. For example, savings can be in the 50–80% range with a rod-shaped crystal that is aligned diagonally with the camera.

In most cases the beam size should conform to the cell size to achieve full coverage of the grid. The default mode is to set the beam size automatically to match the cell size by adjusting the slits or by inserting one of the 5  $\mu\text{m}$ , 10  $\mu\text{m}$  or 20  $\mu\text{m}$  exchangeable mini-beam apertures. There is also an option for manual override of the default.

### 2.2. Data analysis

Diffraction images may optionally be analyzed by the program *DISTL*, which is part of the *LABELIT* package (Zhang *et al.*, 2006). *DISTL* analyzes a single diffraction image quickly and produces several statistics relevant to crystal quality, including total number of diffraction maxima, limiting resolution of the image and number of ice rings.

Diffraction images are processed in parallel with collection using the multiple cores of the workstations that run *JBluIce-EPICS*. Since the workstations have four cores, four processes are spawned at a time. The network and CPU in this configuration can keep up with the collection speed (about 18 images per minute with 1 s exposure times). Raster runs with a high-speed detector could require a different approach to real-time processing.

In the results table of the raster interface, the quality indicators are displayed in columns (Fig. 1). These results may be used to select a cell and center it for fine-step rastering or for data collection. The quality of each cell can also be evaluated by viewing the diffraction images directly.

### 2.3. Multiple run algorithms

The raster interface was designed to be flexible and to allow users to develop methods for finding crystals, initially with a simple rectangular grid to find micro-crystals and center them in the beam. For large crystals, we envisioned that the main use of the raster feature would be to locate the best diffracting site in the sample in three dimensions using a simple three-run protocol and a highly attenuated beam. [Run 1: a coarse-grid raster using a large cell and the full beam size ( $\sim 30 \times 100 \mu\text{m}$ ;  $V \times H$ ) with the sample rotated so the beam intercepts its smallest profile; run 2: a fine-grid raster within the most promising cell from run 1 using a 5  $\mu\text{m}$ , 10  $\mu\text{m}$  or 20  $\mu\text{m}$  mini-beam; and run 3: a fine-grid single-column raster after

selecting the most promising cell in run 2 and rotating the sample by 90° about the horizontal  $\omega$  axis.] Such a protocol could be incorporated into an automated system for screening and data collection. However, GM/CA users immediately requested additional features for the raster that would allow them to tailor raster runs to the peculiarities of their samples.

### 3. Vector collect

Vector collection is an added feature of data collection that allows the user to design a data collection protocol in which the sample is systematically moved to place new parts of the crystal in the beam before radiation damage causes diffraction quality to fall below acceptable levels. The simple vector set-up is performed once at the beginning of collection. This eliminates the need to pause frequently, translate the sample in three dimensions, and re-center it.

Vector collection can be used on any crystal that is large enough to be intercepted at two or more non-overlapping positions by an X-ray beam of the desired size. Rod-shaped crystals oriented almost along the rotation axis are an ideal case for the vector collect feature because, as the crystal translates and rotates, the beam intercepts a consistent volume of crystal. However, the vector collect feature can be of benefit for a crystal of any shape or orientation in which the projection of crystal length onto the rotation axis is substantially larger than the beam width.

The vector collect feature can also be used to map crystal quality along an arbitrary direction (for example, Jensen *et al.*, 2010). Single low-dose shots will generate diffraction images that can be visually checked to determine which sites on the sample are best for data collection as a function of both sample rotation and translation along the vector.

Crystal translation during data collection was shown to improve data quality in the helical data collection at the ESRF (Flot *et al.*, 2010). Specifically, the profile of scaling  $B$ -factor across the rotation range was much flatter when compared with non-vector collection, consistent with a reduction in the effects of radiation damage, and a significant signal-to-noise improvement helped all data quality indicators. These observations apply to our implementation as well, which differs from previous works by full user control of the data-collection protocol. Many GM/CA users take advantage of the vector-collect feature, particularly for highly radiation-sensitive crystals (Rasmussen *et al.*, 2011; Rosenbaum *et al.*, 2011).

#### 3.1. Vector collect use

To set the vector position, the two endpoints are defined in the vector-collect interface and displayed along with the vector length (Fig. 2). Using the camera controls, each endpoint can be centered on the crosshair (beam position) and saved. The endpoints can also be accurately defined by limited raster scans around the ends of the crystal.

Four parameters specified by the user define where each diffraction image will be taken along a given vector. The first data-collection site is located at the vector start point. The first

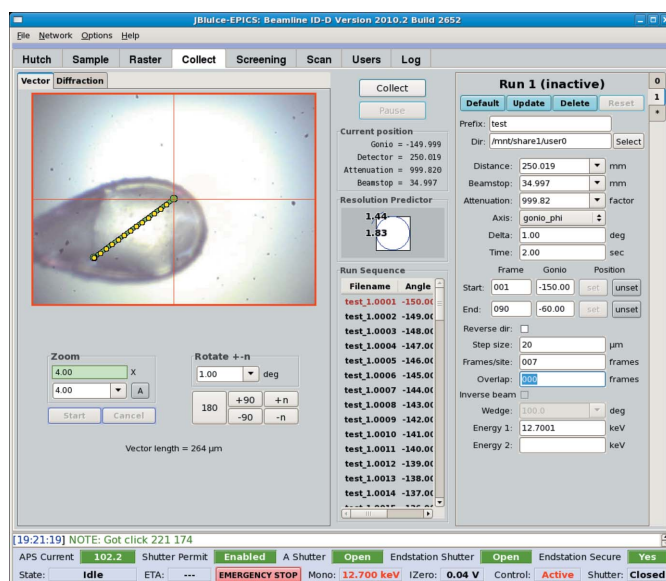


**Figure 2**

Vector collect set-up. In this experiment, data collection is set up along a three-dimensional vector at 13 sites with 20  $\mu\text{m}$  separation, appropriate for data collection with a 5  $\mu\text{m}$  or 10  $\mu\text{m}$  mini-beam. A total of 90 diffraction images, each of 1° crystal rotation, will be recorded, seven diffraction images from each site along the vector except for the last.

parameter, ‘distance’, is the separation in micrometer units between sites along the vector. The second parameter, ‘frames per site’, defines the number of diffraction images to be taken at each site. The third parameter, ‘overlap’, defines the number of diffraction images recorded at the previous site to be repeated at each fresh site in order to facilitate data processing and scaling. Finally, a ‘reverse’ parameter can swap the vector endpoints without the need to redefine the points.

#### 3.2. Vector collect implementation

The  $x$ ,  $y$ ,  $z$  motor positions for each collection site are calculated based on the vector endpoints and the four parameters described in §3.1. During data collection, for each new collection site the three motors are moved to the positions that are calculated for that site. Then, the sample is rotated on the goniometer during the image acquisition according to the standard (non-vector) run settings, for the appropriate number of diffraction images per site. The vector collect feature is fully integrated with the *JBluIce-EPICS* collect tab, and appears as both a sub-tab as well as associated run fields.

### 4. Conclusions and future work

The automated sample-scanning algorithms that have been added to *JBluIce-EPICS* enable efficient data collection from invisible crystals and improve data quality by systematically moving a fresh crystal volume into the beam. At the same time, these tools decrease the time required by the user to probe crystals with mini-beams, which allows users to focus on other aspects of the experiment. These advantages combine to significantly increase user productivity and have been extre-

mely well received by users with crystals that are tiny, invisible, inhomogeneous or radiation-sensitive. More extensive use of the raster feature would be enabled by a faster detector, which would allow for slew diffraction rastering but would require a load-balancing compute cluster for real-time processing of diffraction images. For example, frame rates exceeding  $2\text{ s}^{-1}$  have been achieved in diffraction rastering with a Pilatus detector at the Diamond Light Source, where a multi-CPU cluster runs *DISTL* to return quality indicators in under 5 s (Aishima *et al.*, 2010). Combining slew and polygon diffraction rastering will be a useful further development of the method since slewing provides a higher frame rate while polygon rastering reduces the number of diffraction images needed to characterize the sample.

The raster and vector collect features depend critically on a high degree of reproducibility and stability in the beamline optics, the beam delivery and the sample-positioning systems, which together allow a sample to be positioned repeatedly to within  $1\text{ }\mu\text{m}$  and the beam size to be changed rapidly, reliably and on demand (Fischetti *et al.*, 2009). After introduction of a mini-beam under computer control, GM/CA users immediately used it to probe a variety of 'poor quality' sample types, and solved structures for many (Rasmussen *et al.*, 2007; Cherezov *et al.*, 2007; Rosenbaum *et al.*, 2007; Hanson *et al.*, 2008; Bokoch *et al.*, 2010). It quickly became apparent that users wanted an adaptable probe that they could tailor to the peculiarities of not only each project but also each sample. Users were generous and enthusiastic with ideas for an adaptable probe. The raster and vector collect features presented here incorporate many user and staff suggestions and considerable testing.

Integration of the raster and vector collect features into the familiar *BluIce* interface facilitates their use and follows our goal of keeping the interface as familiar as possible by introducing new capabilities with the minimum number of new elements and making those elements work as expected by those already familiar with the *BluIce* user interface.

In the future, the raster tab will pass the coordinates of promising sites on the sample to the *JBluIce-EPICS* collect tab for subsequent data collection. Higher levels of automation will be added to the raster feature, for example to execute multiple grid searches with a single click, compiling a list of promising sites for collection. Later, this automatic mode can be incorporated into sample screening which, when combined with automatic strategy calculations, can yield full data collection from a dewar of samples in an unattended mode.

We thank GM/CA CAT users and especially Peter Kuhn and colleagues (The Scripps Research Institute) for helpful discussions and feedback. GM/CA CAT is supported by the National Cancer Institute (Y1-CO-1020) and the National Institute of General Medical Science (Y1-GM-1104) of the NIH. Use of the Advanced Photon Source was supported by the US Department of Energy, Basic Energy Sciences, Office of Science, under contract No. DE-AC02-06CH11357.

## References

- Aishima, J., Owen, R. L., Axford, D., Shepherd, E., Winter, G., Levik, K., Gibbons, P., Ashton, A. & Evans, G. (2010). *Acta Cryst.* **D66**, 1032–1035.
- Bokoch, M. P., Zou, Y., Rasmussen, S. G., Liu, C. W., Nygaard, R., Rosenbaum, D. M., Fung, J. J., Choi, H. J., Thian, F. S., Kobilka, T. S., Puglisi, J. D., Weis, W. I., Pardo, L., Prosser, R. S., Mueller, L. & Kobilka, B. K. (2010). *Nature (London)*, **463**, 108–112.
- Bowler, M. W., Guijarro, M., Petitdemange, S., Baker, I., Svensson, O., Burghammer, M., Mueller-Dieckmann, C., Gordon, E. J., Flot, D., McSweeney, S. M. & Leonard, G. A. (2010). *Acta Cryst.* **D66**, 855–864.
- Caffrey, M. & Cherezov, V. (2009). *Nat. Protocols*, **4**, 706–731.
- Cherezov, V., Hanson, M. A., Griffith, M. T., Hilgart, M. C., Sanishvili, R., Nagarajan, V., Stepanov, S., Fischetti, R. F., Kuhn, P. & Stevens, R. C. (2009). *J. R. Soc. Interface*, **6**, S587–S597.
- Cherezov, V., Rosenbaum, D. M., Hanson, M. A., Rasmussen, S. G., Thian, F. S., Kobilka, T. S., Choi, H. J., Kuhn, P., Weis, W. I., Kobilka, B. K. & Stevens, R. C. (2007). *Science*, **318**, 1258–1265.
- Chien, E. Y., Liu, W., Zhao, Q., Katritch, V., Han, G. W., Hanson, M. A., Shi, L., Newman, A. H., Javitch, J. A., Cherezov, V. & Stevens, R. C. (2010). *Science*, **330**, 1091–1095.
- Fischetti, R. F., Xu, S., Yoder, D. W., Becker, M., Nagarajan, V., Sanishvili, R., Hilgart, M. C., Stepanov, S., Makarov, O. & Smith, J. L. (2009). *J. Synchrotron Rad.* **16**, 217–225.
- Fischetti, R. F., Yoder, D. W., Xu, S., Stepanov, S., Makarov, O., Benn, R., Corcoran, S., Diete, W., Schwoerer-Boehing, M., Signorato, R., Schroeder, L., Berman, L., Viccaro, P. J. & Smith, J. L. (2007). *Synchrotron Radiation Instrumentation: Ninth International Conference on Synchrotron Radiation Instrumentation*, edited by J.-Y. Choi and S. Rah, pp. 754–757. New York: American Institute of Physics.
- Flot, D., Mairs, T., Giraud, T., Guijarro, M., Lesourd, M., Rey, V., van Brussel, D., Morawe, C., Borel, C., Hignette, O., Chavanne, J., Nurizzo, D., McSweeney, S. & Mitchell, E. (2010). *J. Synchrotron Rad.* **17**, 107–118.
- Gabadinho, J., Beteva, A., Guijarro, M., Rey-Bakaikoa, V., Spruce, D., Bowler, M. W., Brockhauser, S., Flot, D., Gordon, E. J., Hall, D. R., Lavault, B., McCarthy, A. A., McCarthy, J., Mitchell, E., Monaco, S., Mueller-Dieckmann, C., Nurizzo, D., Ravelli, R. B. G., Thibault, X., Walsh, M. A., Leonard, G. A. & McSweeney, S. M. (2010). *J. Synchrotron Rad.* **17**, 700–707.
- Gehret, J. J., Gu, L., Gerwick, W. H., Wipf, P., Sherman, D. H. & Smith, J. L. (2011). *J. Biol. Chem.* **286**, 14445–14454.
- Hanson, M. A., Cherezov, V., Griffith, M. T., Roth, C. B., Jaakola, V. P., Chien, E. Y., Velasquez, J., Kuhn, P. & Stevens, R. C. (2008). *Structure*, **16**, 897–905.
- Jaakola, V. P., Griffith, M. T., Hanson, M. A., Cherezov, V., Chien, E. Y., Lane, J. R., Ijzerman, A. P. & Stevens, R. C. (2008). *Science*, **322**, 1211–1217.
- Jensen, L. M., Sanishvili, R., Davidson, V. L. & Wilmot, C. M. (2010). *Science*, **327**, 1392–1394.
- Leonard, T. A., Rózycki, B., Saidi, L. F., Hummer, G. & Hurley, J. H. (2011). *Cell*, **144**, 55–66.
- McPhillips, T. M., McPhillips, S. E., Chiu, H.-J., Cohen, A. E., Deacon, A. M., Ellis, P. J., Garman, E., Gonzalez, A., Sauter, N. K., Phizackerley, R. P., Soltis, S. M. & Kuhn, P. (2002). *J. Synchrotron Rad.* **9**, 401–406.
- Rasmussen, S. G., Choi, H. J., Fung, J. J., Pardon, E., Casarosa, P., Chae, P. S., Devree, B. T., Rosenbaum, D. M., Thian, F. S., Kobilka, T. S., Schnapp, A., Konetzki, I., Sunahara, R. K., Gellman, S. H., Pautsch, A., Steyaert, J., Weis, W. I. & Kobilka, B. K. (2011). *Nature (London)*, **469**, 175–180.
- Rasmussen, S. G., Choi, H. J., Rosenbaum, D. M., Kobilka, T. S., Thian, F. S., Edwards, P. C., Burghammer, M., Ratnala, V. R., Sanishvili, R., Fischetti, R. F., Schertler, G. F., Weis, W. I. & Kobilka, B. K. (2007). *Nature (London)*, **450**, 383–387.

- Rosenbaum, D. M., Cherezov, V., Hanson, M. A., Rasmussen, S. G., Thian, F. S., Kobilka, T. S., Choi, H. J., Yao, X. J., Weis, W. I., Stevens, R. C. & Kobilka, B. K. (2007). *Science*, **318**, 1266–1273.
- Rosenbaum, D. M., Zhang, C., Lyons, J. A., Holl, R., Aragao, D., Arlow, D. H., Rasmussen, S. G., Choi, H. J., Devree, B. T., Sunahara, R. K., Chae, P. S., Gellman, S. H., Dror, R. O., Shaw, D. E., Weis, W. I., Caffrey, M., Gmeiner, P. & Kobilka, B. K. (2011). *Nature (London)*, **469**, 236–240.
- Sanishvili, R., Nagarajan, V., Yoder, D., Becker, M., Xu, S., Corcoran, S., Akey, D. L., Smith, J. L. & Fischetti, R. F. (2008). *Acta Cryst. D***64**, 425–435.
- Sanishvili, R., Yoder, D. W., Pothineni, S. B., Rosenbaum, G., Xu, S., Vogt, S., Stepanov, S., Makarov, O. A., Corcoran, S., Benn, R., Nagarajan, V., Smith, J. L. & Fischetti, R. F. (2011). *Proc. Natl Acad. Sci. USA*, **108**, 6127–6132.
- Song, J., Mathew, D., Jacob, S. A., Corbett, L., Moorhead, P. & Soltis, S. M. (2007). *J. Synchrotron Rad.* **14**, 191–195.
- Stepanov, S., Makarov, O., Hilgart, M., Pothineni, S. B., Urakhchin, A., Devarapalli, S., Yoder, D., Becker, M., Ogata, C., Sanishvili, R., Venugopalan, N., Smith, J. L. & Fischetti, R. F. (2011). *Acta Cryst. D***67**, 176–188.
- Wu, B., Chien, E. Y., Mol, C. D., Fenalti, G., Liu, W., Katritch, V., Abagyan, R., Brooun, A., Wells, P., Bi, F. C., Hamel, D. J., Kuhn, P., Handel, T. M., Cherezov, V. & Stevens, R. C. (2010). *Science*, **330**, 1066–1071.
- Xu, F., Wu, H., Katritch, V., Han, G. W., Jacobson, K. A., Gao, Z. G., Cherezov, V. & Stevens, R. C. (2011). *Science*, **332**, 322–327.
- Zhang, Z., Sauter, N. K., van den Bedem, H., Snell, G. & Deacon, A. M. (2006). *J. Appl. Cryst.* **39**, 112–119.